

ACTIVE FLOW CONTROL OF FLOW OVER A STATIONARY CYLINDER USING A FLAPPING ROD AT LOW REYNOLDS NUMBER

Ming Han Chua^{1,2}, Bin Liu^{2,3,*}

¹Engineering Cluster, Singapore Institute of Technology, Singapore

²Faculty of Science, Agriculture, and Engineering, Newcastle University, United Kingdom

³Newcastle Research & Innovation Institute (NewRIIS), Singapore

ABSTRACT

A numerical investigation of the active flow control mechanism of flow over a stationary circular cylinder using a flapping rod was conducted at low Reynolds number. The Galerkin-least-square (GLS) stabilized Finite Element formulation in Arbitrary Lagrangian-Eulerian (ALE) description is employed to investigate the fluid dynamics and structural motions in the simulations. A rotating dynamic mesh model is utilized to precisely trace the flapping dynamics of the control rod in the wake downstream. A control rod of very small diameter ($d=0.1$) is used as an active flow control mechanism and flaps behind a cylinder ($D=1.0$) in an orbital manner at a range of frequencies, amplitudes, and distance. The primary objective of this study is to investigate the effectiveness of this flapping rod to enhance the structural stability of the cylinder subject to hydrodynamic forces. The results show that this active flow control mechanism, flapping control rod, can effectively change the wake modes downstream and enhance the structural stability by minimizing the fluctuation of lift force.

Keywords: Active Flow Control, Flapping control rod, Galerkin-least-square (GLS) stabilized FEM, Lift Suppression

NOMENCLATURE

VIV	Vortex-induced vibration
GLS	Galerkin-least square
PSPG	Pressure Stabilizing Petrov Galerkin
FEM	Finite element method
ALE	Arbitrary-Lagrangian-Eulerian
Re	Reynolds number
APG	Adverse pressure gradient
VG	Vortex generator
ODE	Ordinary differential equation
LBB	Ladyzhenskaya-Babuska-Brezzi

*Corresponding author: bin.liu@newcastle.ac.uk

1. INTRODUCTION

Boundary layer transition and separation phenomena have been researchable topics for over 100 years, but there are still many open essential issues and practical challenges containing their controls. It is predicted that the fuel cost of a commercial aircraft could be saved to 8% if the transition phenomenon over its wing could be delayed to 50% [1]. These flow phenomena commonly occur at low Reynolds numbers (Re) at which laminar flow is dominant. A laminar boundary layer can separate from the solid surface when the adverse pressure gradients (APGs) play a preponderant role. It is believed APG is one of the important driving force of flow separation and manifests the fundamental mechanism of hydrodynamic instabilities developed in the boundary layer. Subsequently transition phenomenon in the separated region is caused by the separated shear layer, and then the turbulent reattachment starts to occur because of energized vortical structures.

The flow separation generally implies a bad sign of hydrodynamic stability and induces the chaotic nature of fluid dynamics, e.g., loss of lift & increased drag, stalling, vortex shedding and buffeting, reduced efficiency (large energy dissipation), and induced structural instability, e.g., vortex-induced vibration (VIV), galloping and fluttering, for the submerged bluff bodies. To deal with these critical issues of hydrodynamic/structural stability, a number of flow control mechanisms were developed over decades. Nonetheless the flow control methods can still be broadly categorized into passive and active approaches. The passive flow control mechanism, such as the use of dimples on golf balls or vortex generators on aircraft wings, rely on structural modifications to influence flow characteristics. On the other hand, active flow control mechanism involves the input of energy into the system, such as through the use of jets, suction/blowing, or structural dynamics, to manipulate the topology of velocity field associated with flow features. The choice between passive and active methods depends on the application, desired outcomes, and resource

availability.

The passive flow control mechanism usually manipulates the flow characteristics in the boundary layer and delay the occurrence of boundary layer separation and control mixing in the separated shear layer. The vortex generator (VG) [2] is one of the most effective and simplest passive flow control device that are widely used on wind turbine blades by aerodynamic researchers in order to prohibit and suppress flow separation caused by APGs. VG examples are not limited to airfoil [3], and they can also utilize the devices such as bluff bodies [4], noise reduction [5], wind turbines [6], swept wings [7], and heat exchangers [8, 9], just to name a few. Other well-established passive flow control mechanism include leading edge vanes [2], leading-edge serrations [10, 11], slotted airfoil [12], splitter plates [13, 14] and roughness material [15].

Active flow control mechanism involves actuators to consume power [16] to inject momentum targeted at the boundary layer to control separation and reduce drag [17]. An actuator's control authority is often highly correlated with its momentum flux or thrust. This contrasts with the passive flow control mechanism, which relies on structural modifications. active flow control techniques are diverse, ranging from the use of synthetic jets, fluidic oscillators, to boundary layer suction and blowing. The primary objective is to delay flow separation, reduce drag, control vortex shedding, and enhance lift. It has emerged as a pivotal area of research in fluid dynamics, offering innovative ways to manipulate flow behavior for enhanced performance in aerospace, automotive, and energy sectors. Some of the most popular active flow control mechanism include synthetic jet actuators [18], plasma actuators [19], rotating control rod [20, 21], flapping plate [22–24], thermal effect [25], and magnus effect [26, 27].

In many engineering applications, the vortex shedding is one of the primary causes inducing the vibrations of the submerged offshore and aeronautical structures. The periodic and alternative shedding vortices from either side of the structure causes a significant fluctuation of hydrodynamic forces, lift and drag. As long as the frequency of these forces get close to the natural frequency of the submerged structure, the resonance may happen eventually, e.g., onset of lock-in in VIV and galloping due to the asymmetric hydrodynamic forces at high reduced velocities. It is known that the vortex shedding of a circular cylinder can be suppressed by the appropriate positioning of a smaller control rod in the near wake [28], though only at very low Reynolds numbers. At higher Reynolds numbers, the flow past bluff shapes, as well as lifting airfoils, can be effectively controlled for drag reduction by adding small control cylinders that are rotated rapidly [29]. The control cylinders, when placed in close proximity to a bluff body and rotated at high rates, interact with the separating boundary layer to cause it to reattach and reduce pressure drag. The drag reduction is sensitive to the control cylinder position, diameter, and normalized surface speed, $\xi = u_{surf}/U_\infty$. Here, u_{surf} is the tip speed of the control cylinder and U_∞ is the free-stream velocity. Wu and Shu (2011) [22] found that by attaching a flapping rigid plate behind a circular cylinder, the drag force exerted on the cylinder can be reduced effectively and the vortex shedding process can be significantly alleviated and suppressed. They also identified two distinct vortex interaction modes-constructive interaction and de-

structive interaction. These modes offer insights into the complex dynamics of fluid flow in the presence of a flapping plate. On the other hand, besides a splitter plate, Strykowski & Sreenivasan (1990) [28] and Dipankar & Sengupta, etc. (2004) [30] also found that by placing a control rod in the wake behind a cylinder can significantly suppress the vortex shedding and formation. More recently, the flow control mechanism using vibrating, rotating, or stationary control rod(s) in the vicinity of cylinder has gain significant attention in the community of fluid dynamics. For instance, Wu & Wang (2020) [31] conducted numerical simulation of VIV of circular cylinder with two control rods and found that the rods suppress and enhance VIV if the position angle α is less or greater than 90° , respectively. Increasing number of control rods can improve VIV suppression effectiveness. Song et al. (2017) [32] conducted numerical simulations of the suppression of VIV of a circular cylinder surrounded by three control rods in an equilateral triangle arrangement and found that the best VIV suppression occurred when the arrangement angle was $\alpha = 45^\circ$, a slightly oblique attack case. Liu et al. (2022) [33] conducted numerical simulation of VIV of a circular cylinder and increase the number of control rods to 6 in a hexagon arrangement.

In this study, combining the features of both flapping plate and stationary control rod, a flapping control rod is proposed as an active flow control mechanism. In contrast to the flapping rigid plate, the flapping control rod is much more smaller in size and consume less energy during actuation. The primary objective is to allow the flapping motion of the control rod to influence the frequency and fluctuation of hydrodynamic forces. The numerical study is conducted at Reynolds number 100. The size of the control rod is chosen as 1/10 of the cylinder. The control rod flaps at a range of frequency, amplitude and distance behind the cylinder.

The structure of this article is arranged as follow: The formulations of numerical method are presented in Section 2. The description of computational domain and validation cases are provided in Section 3. The numerical results are presented and discussed in Section 4. Finally, the conclusions are drawn in Section 5.

2. NUMERICAL METHODS

2.1 Governing equations

The governing equations of unsteady incompressible Navier-Stokes equation are written in Equation (1).

$$\rho(\partial_t \mathbf{u} + (\mathbf{u} \cdot \nabla) \mathbf{u}) = \nabla \cdot \boldsymbol{\sigma}\{\mathbf{u}, p\} \quad \forall \mathbf{x} \in \Omega^f(t) \quad (1a)$$

$$\nabla \cdot \mathbf{u} = 0 \quad \forall \mathbf{x} \in \Omega^f(t) \quad (1b)$$

$$\mathbf{u} = \tilde{\mathbf{u}} \quad \forall \mathbf{x} \in \Gamma_D^f(t) \quad (1c)$$

$$\boldsymbol{\sigma}\{\mathbf{u}, p\} \cdot \mathbf{n} = \tilde{\mathbf{h}} \quad \forall \mathbf{x} \in \Gamma_N^f(t) \quad (1d)$$

$$\mathbf{u} = \tilde{\mathbf{u}}_0 \quad \forall \mathbf{x} \in \Omega^f(0) \quad (1e)$$

where ρ , \mathbf{u} , \mathbf{u}_0 , $\tilde{\mathbf{u}}$, $\tilde{\mathbf{h}}$ and \mathbf{n} are respectively the fluid density, the fluid velocity vector, the initial fluid velocity vector, the prescribed fluid velocity, the prescribed fluid traction force and the outward normal vector of fluid domain. The superscript (f) refers to the quantity related to the fluid flow. Based on the

kinematics of continuum mechanics, the left-hand-side of Equation (1a) can be written as the material time derivative $D_t(\rho\mathbf{u})$. It describes the kinematics of a fluid particle in Lagrangian description. The term $\partial_t(\cdot)$ refers to the time derivative of a variable with respect to the spatial coordinates (\mathbf{x}). On the other hand, in accordance to the Newton's second law, the right-hand-side of Equation (1a) represents the total external force exerted on this fluid particle. The gravitational field is a conservative potential field, $\mathbf{g} = -\nabla\phi = [0, -g, 0]^T = [0, -9.81, 0]^T$. Hence it is combined with the hydrostatic pressure (p_{stat}) to form a modified pressure field, $p = p_{stat} + \rho\phi$, in Equation (1a). It should be noted that the hydrostatic pressure is equivalent to thermodynamic pressure for incompressible Newtonian fluid flow. In other word, the gravitational effect, e.g., fluid free interface, and other non-conservative external forces are out of the scope of discussion. In the rest of this article, the modified pressure is simply referred to as fluid pressure. Consequently, the fluid particle is assumed to be driven merely by the viscous stresses, $\nabla \cdot \boldsymbol{\sigma}\{\mathbf{u}, p\}$, in this article, where the Cauchy stress tensor ($\boldsymbol{\sigma}$) is defined as

$$\boldsymbol{\sigma}\{\mathbf{u}, p\} = -p\mathbf{I} + 2\mu\boldsymbol{\epsilon}(\mathbf{u}) \quad (2a)$$

$$\boldsymbol{\epsilon}(\mathbf{u}) = \frac{1}{2}[\nabla\mathbf{u} + (\nabla\mathbf{u})'] \quad (2b)$$

where p , \mathbf{I} , μ and $\boldsymbol{\epsilon}(\mathbf{u})$ respectively are the fluid pressure, the identity matrix, the dynamic viscosity and the strain rate tensor.

2.2 GLS-stabilized finite element formulation

First of all, the numerical formulation is derived by spatially discretizing the governing equations of their primitive variables in Equation (1) using a GLS-stabilized and Pressure Stabilizing Petrov Galerkin (PSPG) [34] finite element formulation [35] to minimize the spurious oscillations (caused by the nonlinear advection term) in fluid velocity field by introducing numerical diffusion and circumventing the Ladyzhenskaya-Babuska-Brezzi (LBB) condition of coupled velocity-pressure field, in which the velocity and pressure fields are approximated using the same order of polynomials. The spatial discretization results in a semi-discrete ordinary differential equation (ODE) in time. In finite element formulations, we define appropriate sets of finite trial solution spaces (S_u^h and S_p^h) for fluid velocity and pressure, and the corresponding finite test function spaces (V_u^h and V_p^h) respectively, where the superscript (h) indicates a finite function space, e.g., $S_u^h \subset S_u$. Hence the stabilized finite element formulation of Equation (1) can be written as: for all $\psi_u^h \in V_u^h, \psi_p^h \in V_p^h$, find $\mathbf{u}^h \in S_u^h, p^h \in S_p^h$ such that Equation (3) is satisfied.

The $\mathcal{B}_G([\psi_u^h, \psi_p^h], [\mathbf{u}^h, p^h])$ term is derived from the unsteady and incompressible Navier-Stokes equation based on the standard Galerkin method in finite element framework. The $\mathcal{B}_S([\psi_u^h, \psi_p^h], [\mathbf{u}^h, p^h])$ is the stabilization term based on the GLS and PSPG formulations. The term $\partial_\tau(\cdot)|_{\mathfrak{X}}$ refers to the spatial time derivative with respect to the fixed referential coordinates (\mathfrak{X}) and the dimensionless time (τ) in ALE description. In Equation (3), the nonlinear incompressible Navier-Stokes equation is linearized by Newton linearization to achieve quadratic convergence, and the solution at each time step is updated in iterations until convergence. The variable \mathbf{u}_n^h refers to the solution

of velocity field in the last iteration. Upon convergence, the term $((\mathbf{u}_n^h - \mathbf{u}_m^h) \cdot \nabla)\mathbf{u}^h + ((\mathbf{u}^h - \mathbf{u}_m^h) \cdot \nabla)\mathbf{u}_n^h - ((\mathbf{u}_n^h - \mathbf{u}_m^h) \cdot \nabla)\mathbf{u}_n^h$ reduces to $((\mathbf{u}^h - \mathbf{u}_m^h) \cdot \nabla)\mathbf{u}^h$. The stabilization parameters (τ_m and τ_c) are defined as

$$\tau_m = \left[\left(\frac{2}{dt} \right)^2 + \left(\frac{2\|\mathbf{u}\|}{h_e} \right)^2 + 9 \left(\frac{4}{Re h_e^2} \right)^2 \right]^{-1/2} \quad (4a)$$

$$\tau_c = \frac{h_e}{2} \|\mathbf{u}\| \gamma \quad \text{for } \gamma = \begin{cases} Re_u/3 & 0 < Re_u \leq 3 \\ 1 & 3 < Re_u \end{cases} \quad (4b)$$

where Re_u and h_e respectively are the local Reynolds number and the size of element. The value of \mathbf{u}_m is the dimensionless mesh velocity in the (rotational) dynamic mesh modal. The second-order accurate and unconditionally stable generalized- α time integration scheme [36–39] is employed to march the numerical solution of Navier-Stokes equation in time.

2.3 Dynamic mesh model

The fluid solver is coupled with the structural solver by satisfying the kinematic and dynamic constraints along the fluid-structure interface (Γ^{fs}), as presented in Equation (5).

$$\mathbf{u}(\Phi(\mathfrak{X}, \tau), \tau) = \partial_\tau \Phi(\mathfrak{X}, \tau) \quad \forall \mathfrak{X} \in \Gamma^{fs}(\tau) \quad (5a)$$

$$\mathbf{h}(\Phi(\mathfrak{X}, \tau), \tau) = -\mathbf{h}^{cyl}(\Phi(\mathfrak{X}, \tau), \tau) \quad \forall \mathfrak{X} \in \Gamma^{fs}(\tau) \quad (5b)$$

where \mathbf{h} and $\mathbf{h}^{cyl} = [h_x^{cyl}, h_y^{cyl}]$ respectively are the dimensionless fluid and structural stresses along the fluid-structure interface. The value of Φ is the dimensionless location of the structure, which is defined in Equation (6), where $\boldsymbol{\eta}$ is the dimensionless displacement of structure at time τ . In this investigation, the referential coordinates can be taken as the initial position of the rigid circular cylinder. The values of $\partial_\tau \Phi$ and $\partial_\tau^2 \Phi$ are defined as the structural velocity and acceleration respectively.

$$\Phi(\mathfrak{X}, \tau) = \boldsymbol{\eta}(\mathfrak{X}, \tau) + \mathfrak{X} \quad \forall \mathfrak{X} \in \Omega^s(\tau) \quad (6)$$

where the superscript (s) indicates the structural variables. In this study, the no-slip boundary condition is imposed along the cylinder. The flapping control rod is under forced motion, in which its angular displacement (flapping angle) and angular velocity in Equation (7) are imposed along the control rod. The \mathcal{A} , \mathcal{T} , and τ refers to the maximum flapping angle, flapping period, and dimensionless time, respectively.

$$\theta = \mathcal{A} \sin\left(\frac{2\pi}{\mathcal{T}} \tau\right) \quad (7a)$$

$$\omega = \frac{\partial \theta}{\partial \tau} = \mathcal{A} \frac{2\pi}{\mathcal{T}} \cos\left(\frac{2\pi}{\mathcal{T}} \tau\right) \quad (7b)$$

In this ALE formulation, the nodal coordinates of dynamic mesh are mapped using a popular bi-harmonic model [40, 41], whose strong form reads as

$$-\nabla \cdot (\alpha_e \nabla \mathbf{d}) = 0 \quad \forall \mathbf{x} \in \Omega^f(\tau) \quad (8)$$

$$\tilde{\mathbf{d}} = \boldsymbol{\eta} \quad \forall \mathbf{x} \in \Gamma^{fs}(\tau)$$

$$\tilde{\mathbf{d}} = \mathbf{0} \quad \forall \mathbf{x} \in \Gamma^f(\tau)/\Gamma^{fs}(\tau)$$

where \mathbf{d} are the dimensionless grid displacement with respect to the fixed referential framework \mathfrak{X} . The value of α_e is a "stiffness parameter" of the mesh.

$$\begin{aligned}
& \underbrace{\int_{\Omega^f} \left[\boldsymbol{\psi}_u^h \cdot \left(\partial_\tau \mathbf{u}^h |_{\mathcal{X}} + ((\mathbf{u}_n^h - \mathbf{u}_m^h) \cdot \nabla) \mathbf{u}^h + ((\mathbf{u}^h - \mathbf{u}_m^h) \cdot \nabla) \mathbf{u}_n^h \right] d\Omega^f \right]}_{\mathcal{B}_G([\boldsymbol{\psi}_u^h, \boldsymbol{\psi}_p^h], [\mathbf{u}^h, p^h])} \\
& \underbrace{\int_{\Omega^f} \left[\boldsymbol{\psi}_u^h \cdot \left(-((\mathbf{u}_n^h - \mathbf{u}_m^h) \cdot \nabla) \mathbf{u}_n^h \right) + \epsilon(\boldsymbol{\psi}_u^h) : \boldsymbol{\sigma}(\mathbf{u}^h, p^h) \right] d\Omega^f}_{\mathcal{B}_G([\boldsymbol{\psi}_u^h, \boldsymbol{\psi}_p^h], [\mathbf{u}^h, p^h])} - \int_{\Gamma_N^f} \boldsymbol{\psi}_u^h \cdot \tilde{\mathbf{h}}^h d\Gamma + \int_{\Omega^f} [\boldsymbol{\psi}_p^h \nabla \cdot \mathbf{u}^h] d\Omega^f \\
& + \sum_{e=1}^{n_{el}} \int_{\Omega^f} \tau_m \left[((\mathbf{u}_n^h - \mathbf{u}_m^h) \cdot \nabla) \boldsymbol{\psi}_u^h - \frac{1}{Re} \nabla^2 \boldsymbol{\psi}_u^h + \nabla \boldsymbol{\psi}_p^h \right] \cdot \left[\partial_\tau \mathbf{u}^h |_{\mathcal{X}} + ((\mathbf{u}_n^h - \mathbf{u}_m^h) \cdot \nabla) \mathbf{u}^h - \frac{1}{Re} \nabla^2 \mathbf{u}^h + \nabla p^h \right] d\Omega^f \\
& \underbrace{+ \sum_{e=1}^{n_{el}} \int_{\Omega^f} \tau_c \left[(\nabla \cdot \boldsymbol{\psi}_u^h) (\nabla \cdot \mathbf{u}^h) \right] d\Omega^f = \mathbf{0}}_{\mathcal{B}_S([\boldsymbol{\psi}_u^h, \boldsymbol{\psi}_p^h], [\mathbf{u}^h, p^h])} \quad \forall [\boldsymbol{\psi}_u^h, \boldsymbol{\psi}_p^h] \in V_u^h \times V_p^h
\end{aligned} \tag{3}$$

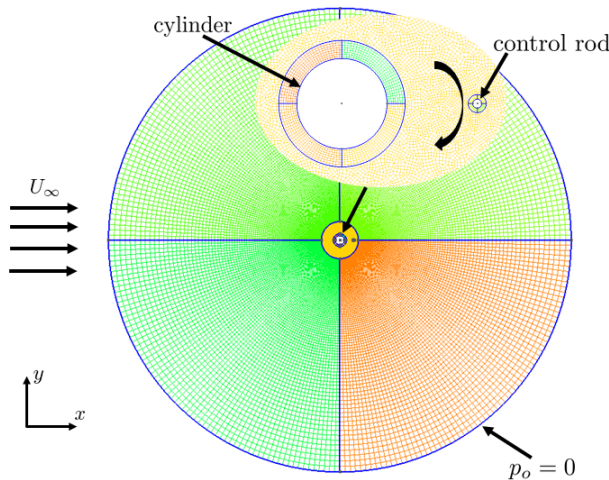


FIGURE 1: Schematic diagram and mesh discretization

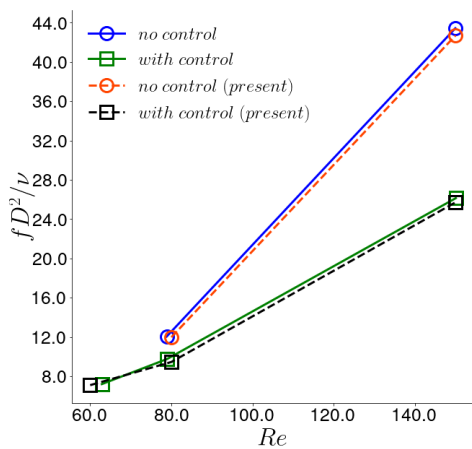


FIGURE 2: Validation of a cylinder with stationary control rod

3. PROBLEM SETUP AND VALIDATION

3.1 Problem setup and boundary conditions

In this study, a circular computational domain is used, as shown in Figure 1. The cylinder is placed on the center of the computational domain, which is also the origin of coordinate system $(x, y) = (0, 0)$. The control rod is initially placed along the center of the cylinder downstream at $x = (l, 0)$, where l is the gap between the cylinder and control rod. The left-half boundary of the circular domain is the inlet. On the other hand, the right-half boundary is the outlet. The fluid flows over the cylinder and control rod from the left to the right. In the proposed active flow control mechanism, the control rod flaps behind the cylinder at a particular frequency (\mathcal{T}) and amplitude (\mathcal{A}). During flapping, the (radial) gap distance between the cylinder and control rod retains constant and the cylinder remains stationary.

The radial distance (the radius) of the circular computational domain is $50D$, where D refers to the diameter of the cylinder. Following literature [28, 30, 42] in which the suppression was found phenomenal, the diameter of the control rod is chosen as $0.1D$. The inlet velocity is $\mathbf{u} = (U_\infty, 0)$ and the referential pressure is pinned at a point along the outer boundary of the computational domain, $p_o = 0$.

There are totally 140 and 50 elements along the surfaces of cylinder and control rod, respectively. The height of first layer of boundary layer mesh is below $y^+ = 1$ to ensure the accuracy of calculated hydrodynamic forces. For the elements further away from the cylinder and control rod, their growth rate is well controlled below 1.1 to alleviate the skewness of the element's shapes and distortion.

3.2 Validation and convergence analysis

The numerical results from the implemented GLS-stabilized finite element formulation have been validated and verified using the canonical cases [43–47], e.g., flow over a stationary cylinder. In this study, a validation is also conducted in the cases of a cylinder with stationary control rod and compared with literature [30],

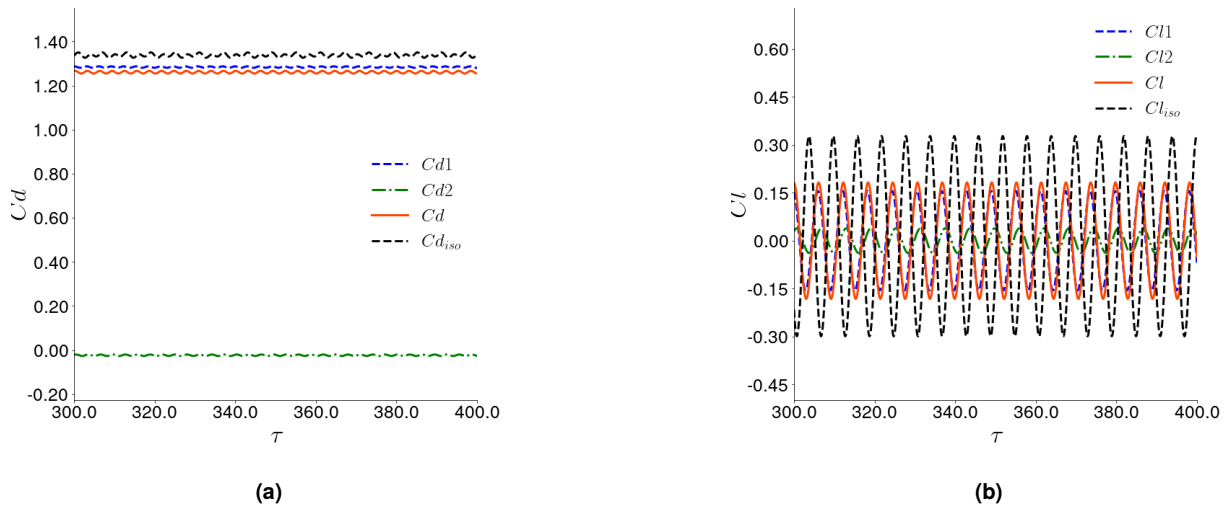


FIGURE 3: Time history of hydrodynamic forces exerted on cylinder with a stationary control rod at $l = 0.5$

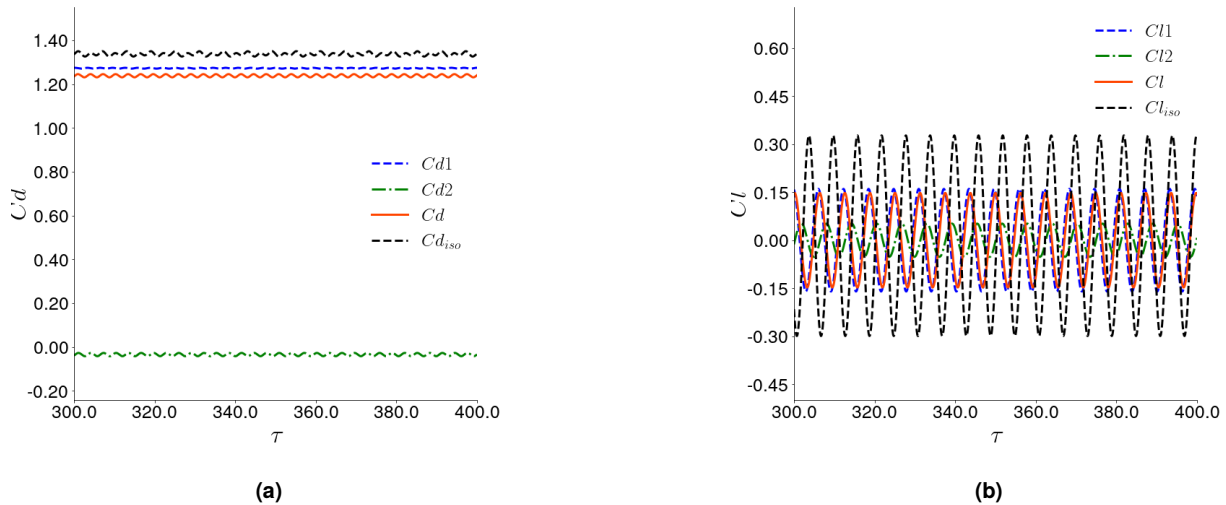


FIGURE 4: Time history of hydrodynamic forces exerted on cylinder with a stationary control rod at $l = 1$

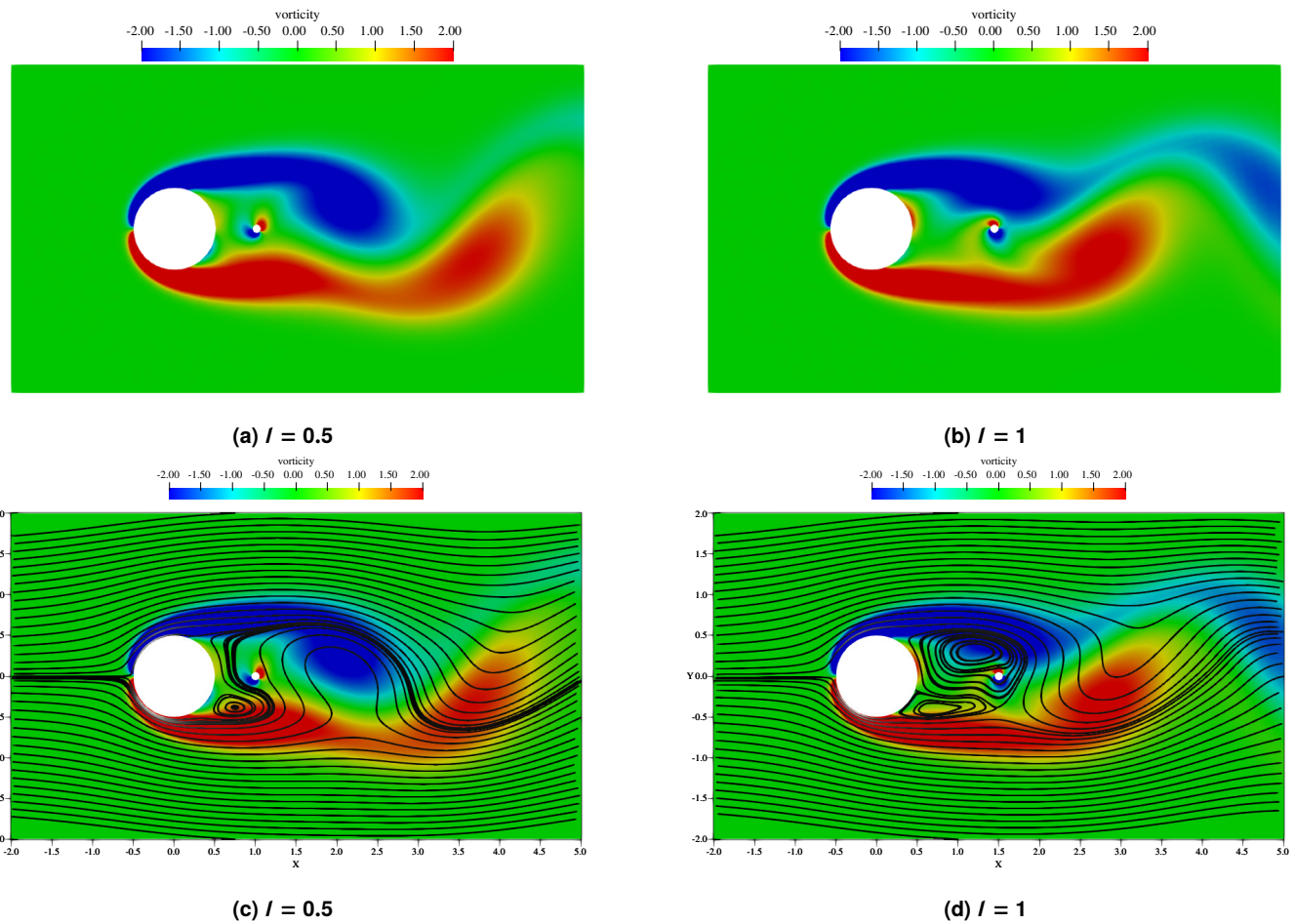


FIGURE 5: Instantaneous contour of vorticity and streamline for the cases at $Re = 100$, and $\tau = 400$: (a, b) vorticity contour and (c, d) streamline

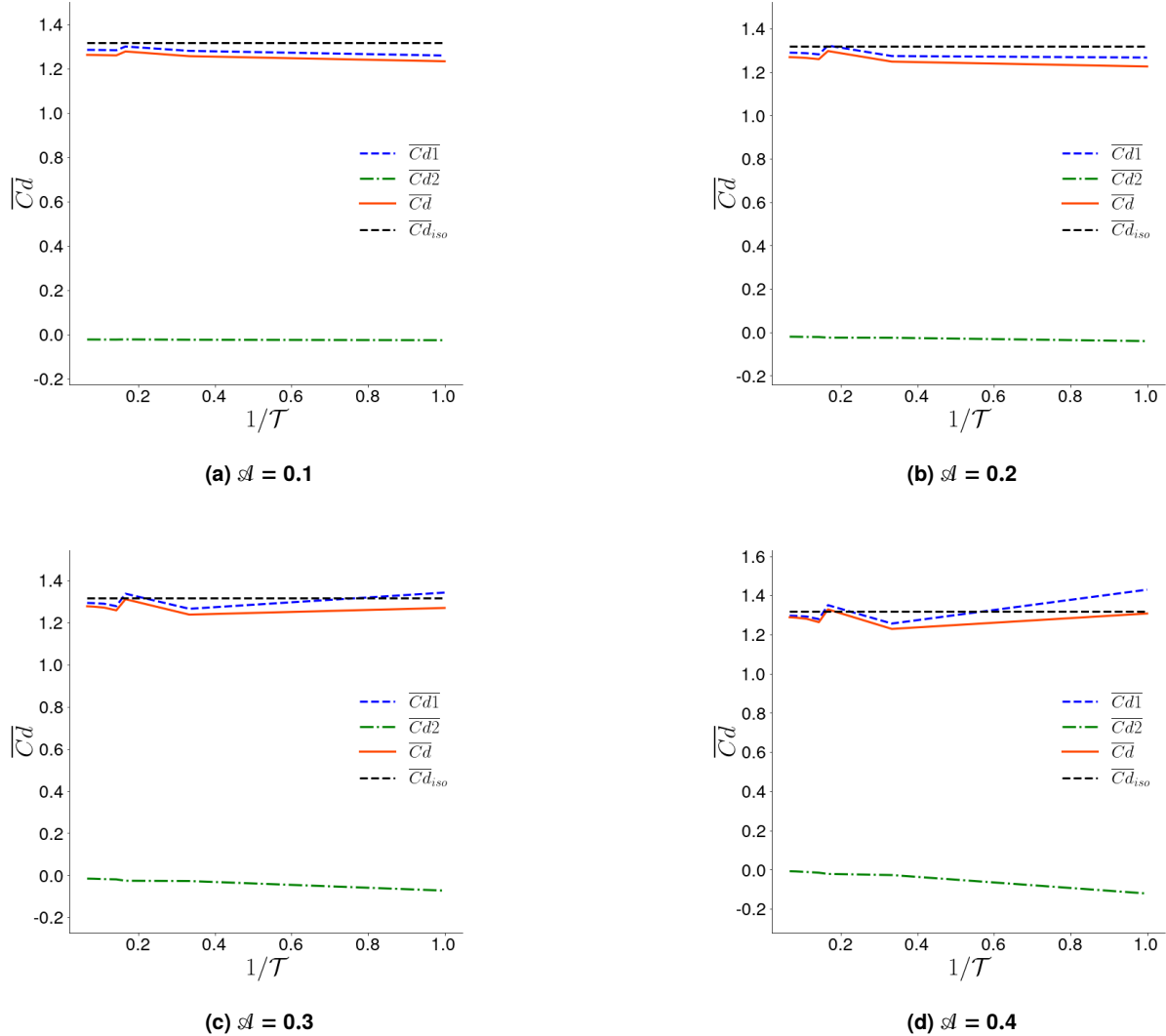


FIGURE 6: Comparison of mean drag forces for the cases with a flapping control rod at $Re = 100$ and $l = 0.5$

TABLE 1: Flow over a cylinder with stationary control rod at Reynolds number 100, $l = 1.0$, and different mesh resolutions

MESH	NODES	$\overline{C_d}$	C_d^{rms}
M3	2.5×10^4	1.345 (0.5%)	0.1075 (1.9%)
M2	4.9×10^4	1.279 (0.0%)	0.1092 (0.4%)
M1	9.4×10^4	1.279	0.1096

as shown in Figure 2. The convergence analysis is shown in Table 1, in which the drag and lift forces refer to the hydrodynamic forces exerted along the cylinder. For all the cases presented in this study, the total number of elements are chosen to be 50000 approximately, and the time step is set at $dt = 0.02$.

4. RESULTS AND DISCUSSION

4.1 Effects of a stationary control rod in wake

Strykowski & Sreenivasan (1990) [28] and Dipankar & Sen-gupta, etc. (2004) [30] noticed that by simply placing a stationary control rod in the wake, the vortex shedding behind a cylinder can be significantly suppressed. This phenomenon is also found in this study. As shown in Figure 3 and Figure 4 respectively, the fluctuation of lift forces are effectively suppressed to 0.16 by placing a stationary control rod at the cylinder-to-rod distance $l = 0.5$ and 1.0. The amplitude of fluctuation of life force in the case of stationary circular cylinder at $Re = 100$ is 0.313 [39], so a 47% reduction of the lift force can be achieved in those cases. Similar to the lift forces, Figure 3a and Figure 4a also show an obvious suppression of fluctuation of the drag force, albeit the mean value of the drag almost remains the same to the case of a cylinder without a control rod in wake, which is $C_d \approx 1.32$ at $Re = 100$.

As the control rod is placed at different locations, $l = 0.5$ and $l = 1.0$, the control rod affects the vortex shedding at different phases of this process. As shown by the case of $l = 0.5$ in Figure 5a, since the control rod is placed too close to the cylinder, it is completely encapsulated in the low-pressure re-circulation region. In the case of $l = 0.5$, it is also found that the shape and stretching of the vorices shed downstream are still intact and regular, similar to what has been reported in the case of stationary cylinder without a control rod, except that vortex formation length is relatively longer. The vortex formation length, the distance from the cylinder surface to the vortex-shedding location in wake, of a circular cylinder at $Re = 100$ is about $1.0D$; where as this distance becomes $1.5D$ approximately in the case with a control rod at $l = 0.5$ as shown in Figure 5c. Because the topology (stretching) of vortices is closely related to its strength (shear stresses), it is believed that the presence of a control rod at this location modulates and minimized the shed vortices and reduced the amplitude of lift force exerted on the cylinder. On the contrary, as we place the control rod further downstream $l = 1.0$, it can be clearly observed 2 facts: (a) shape (stretching) of the shed vortices is obviously modulated as shown in Figure 5b; (b) the vortex formation length becomes shorter instead, $1.0D$ at $l = 1.0$

in Figure 5d. On the other hand, based on the observation in Figure 3b and Figure 4b, the resultant lift force (red color line) is stronger than that on the cylinder (the blue color line) in the case $l = 0.5$ and vice versa in the case of $l = 1.0$. It means that the shedding of vortices from the control rod is approximately in-phase with the vortex shedding from the cylinder in the case of $l = 0.5$; whereas it is generally anti-phase in the case of $l = 1.0$.

4.2 Effect of a flapping rod on drag forces

If the control rod is allowed to move and flap in wake at a particular frequency and amplitude, it is believed that the strength and shape of the vortices shed downstream are going to be modulated severely. To study its influence on drag force, the mean and fluctuation of drag force are defined in Equation (9) and the results are shown in Figure 6, 7, 8 and 9.

$$\begin{aligned}\overline{C_d} &= \frac{1}{n} \sum_{i=1}^n C_d; \quad C_d^{rms} = \sqrt{\frac{1}{n} \sum_{i=1}^n (C_d - \overline{C_d})^2} \\ \delta C_d &= \sqrt{2} C_d^{rms}\end{aligned}\quad (9)$$

In vortex shedding, a dimensionless frequency, Strouhal number (St), is proposed to describe the vortex shedding frequency in flow over a cylinder. In the canonical case of flow over a circular cylinder, it was recorded that the frequencies of lift and drag forces are $St = 0.165$ and $St = 0.33$, respectively, where the frequency of lift force fluctuation is also a manifest of the vortex-shedding frequency. In this study, the dimensionless frequency describing the flapping dynamics of control rod is defined as $1/\mathcal{T}$, where \mathcal{T} refers to the dimensionless period of flapping motion.

By comparing the mean drag force at $l = 0.5$ in Figure 6, it is found that the value of mean drag forces are insensitive to the changes in flapping frequency and flapping amplitude: the mean drag force exerted on the control rod (green lines) are almost zero and the mean drag force exerted on the cylinder does not changes obviously. This is expected, as the control rod at $l = 0.5$ is completely encapsulated inside the low-pressure re-circulation region of the cylinder, the form drag on the control rod should be negligible in those cases. Nonetheless, in the case of large flapping amplitude ($\mathcal{A} \gtrsim 0.3$), as the flapping frequency increases, a thrust force is observed on the control rod and the drag forces on the cylinder increases instead. Two distinct cases are worth studying: they are $1/\mathcal{T} \approx 0.165$ and $1/\mathcal{T} \approx 0.33$, since they match perfectly with the frequencies of lift and drag forces of cylinder. It can be noticed that when the flapping frequency matches that of lift force ($1/\mathcal{T} \approx 0.165$), the mean drag force of cylinder increases abruptly; on the other hand, when the flapping frequency matches that of drag force of cylinder ($1/\mathcal{T} \approx 0.33$), the mean drag force of cylinder reaches its minimum.

Analogous to the trend in mean drag force of cylinder, by placing the control rod at $l = 0.5$, the fluctuation of cylinder's drag force also increase significantly at $1/\mathcal{T} \approx 0.165$ and is suppressed to its minimum at $1/\mathcal{T} \approx 0.33$, as shown in Figure 7. This suppression of fluctuation of drag force is enormous and almost reaches zero. It means that by flapping the control rod (at $l = 0.5$) at a frequency of drag force, the fluctuation of drag

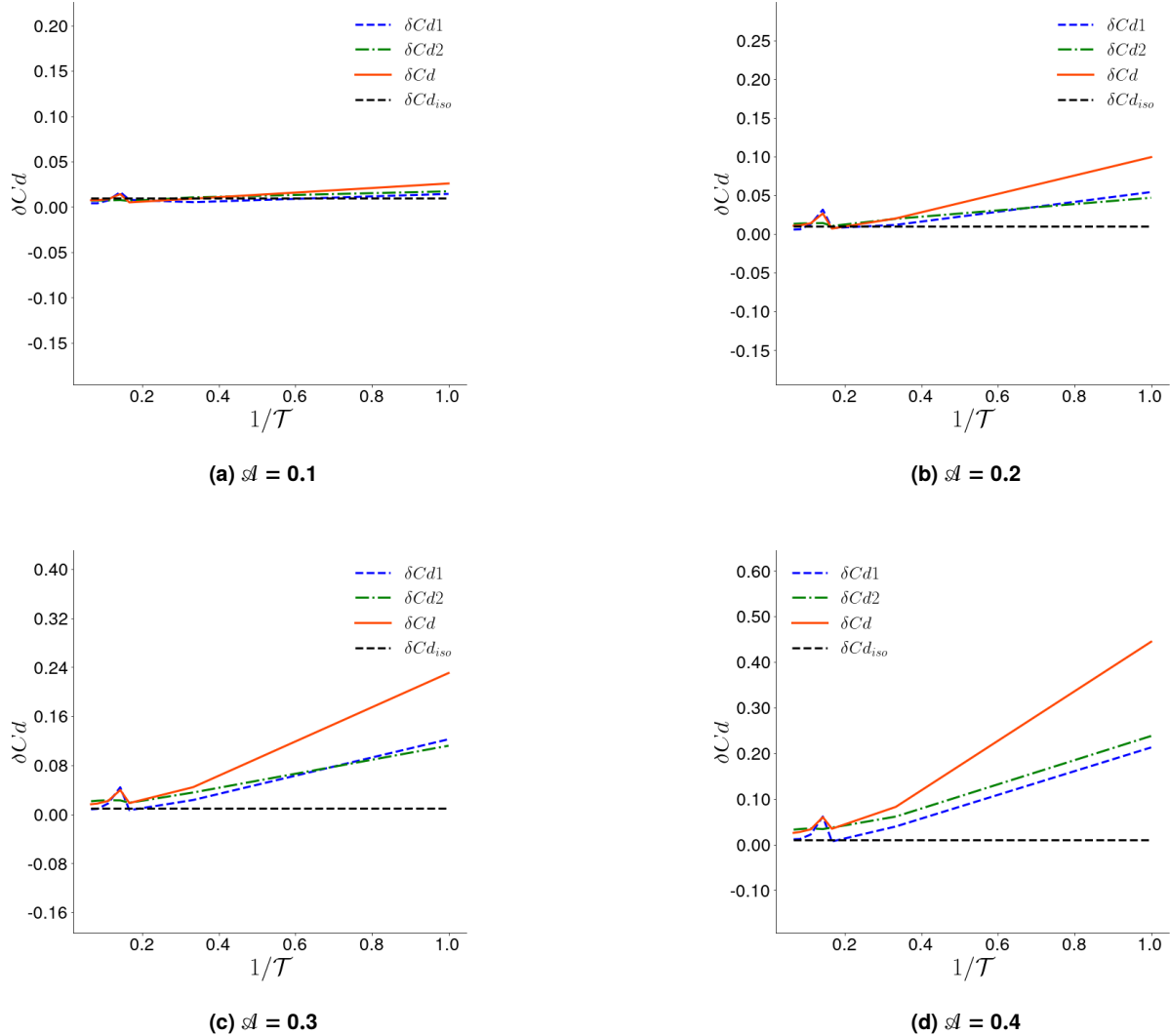


FIGURE 7: Comparison of drag forces fluctuation for the cases with a flapping control rod at $Re = 100$ and $l = 0.5$

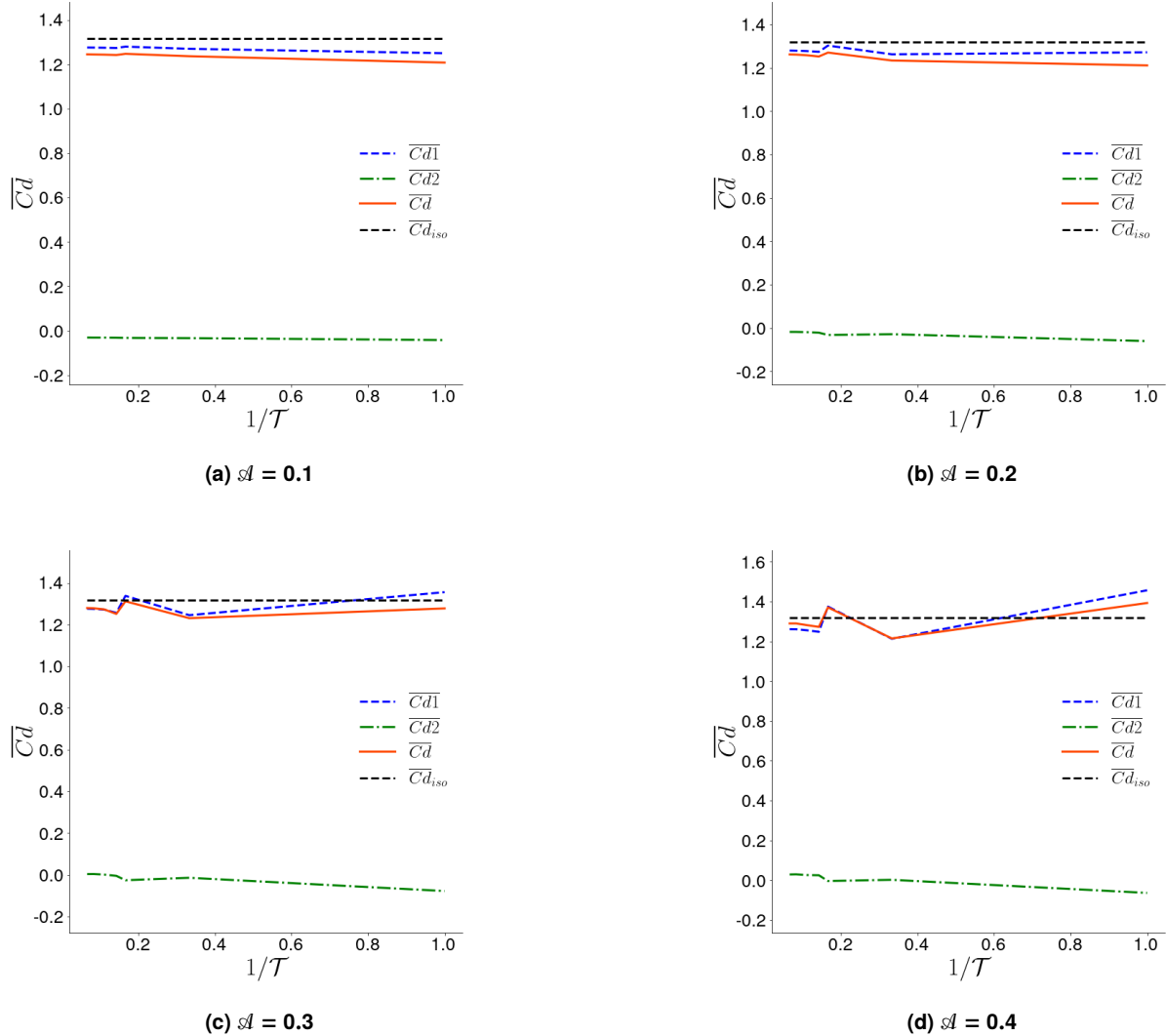


FIGURE 8: Comparison of mean drag forces for the cases with a flapping control rod at $Re = 100$ and $l = 1$

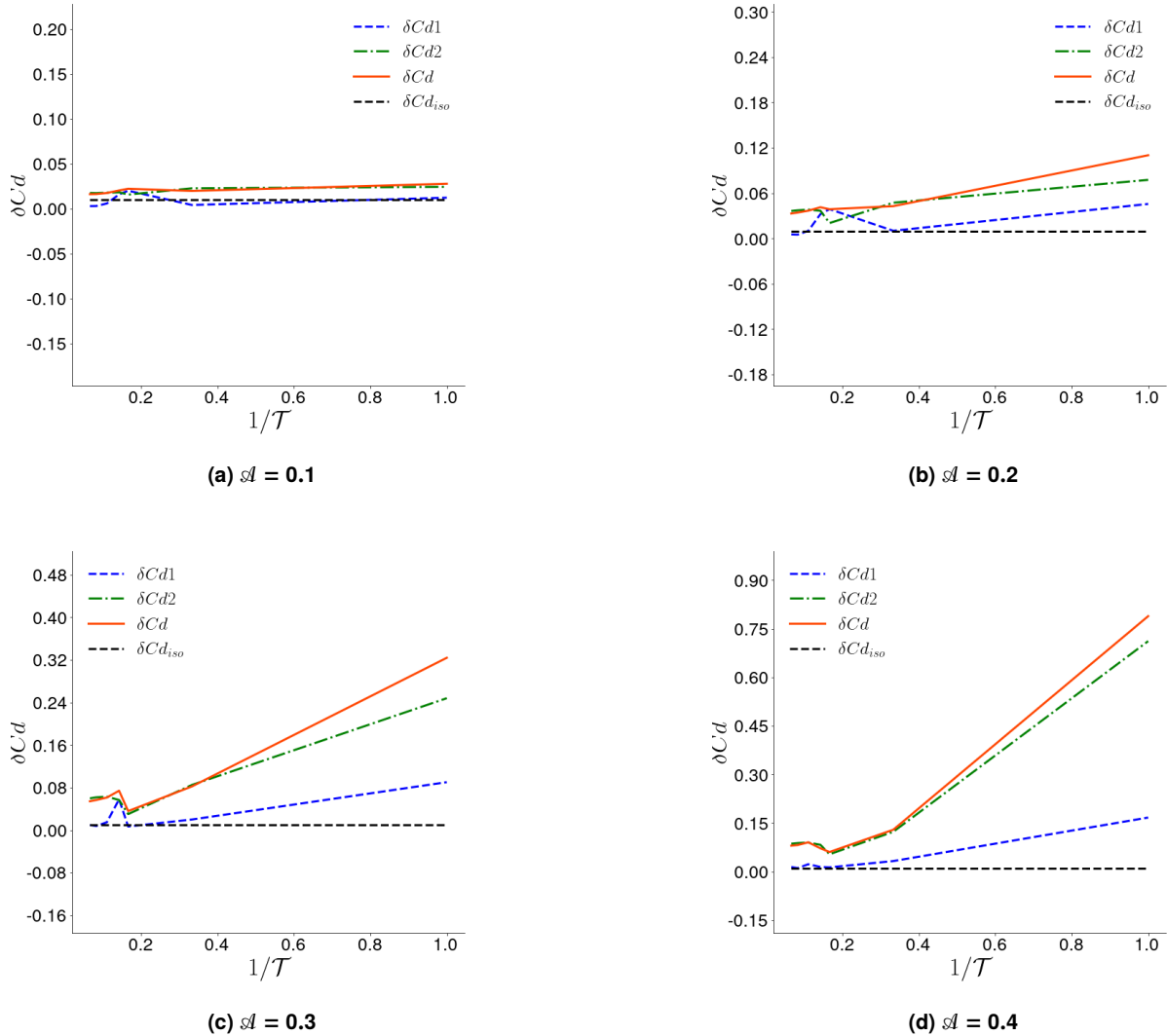


FIGURE 9: Comparison of drag forces fluctuation for the cases with a flapping control rod at $Re = 100$ and $l = 1$

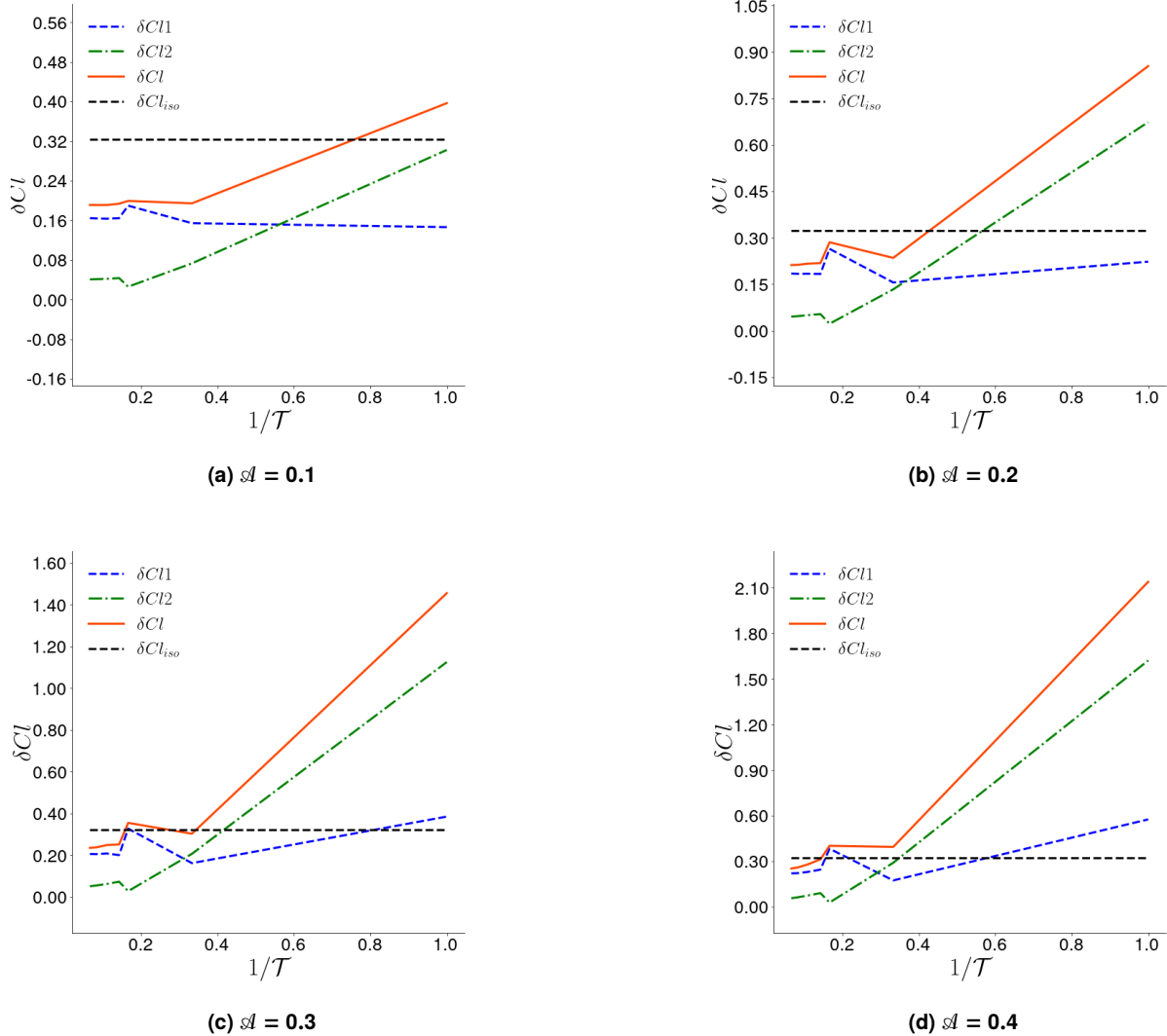


FIGURE 10: Comparison of lift forces fluctuation for the cases with a flapping control rod at $Re = 100$ and $l = 0.5$

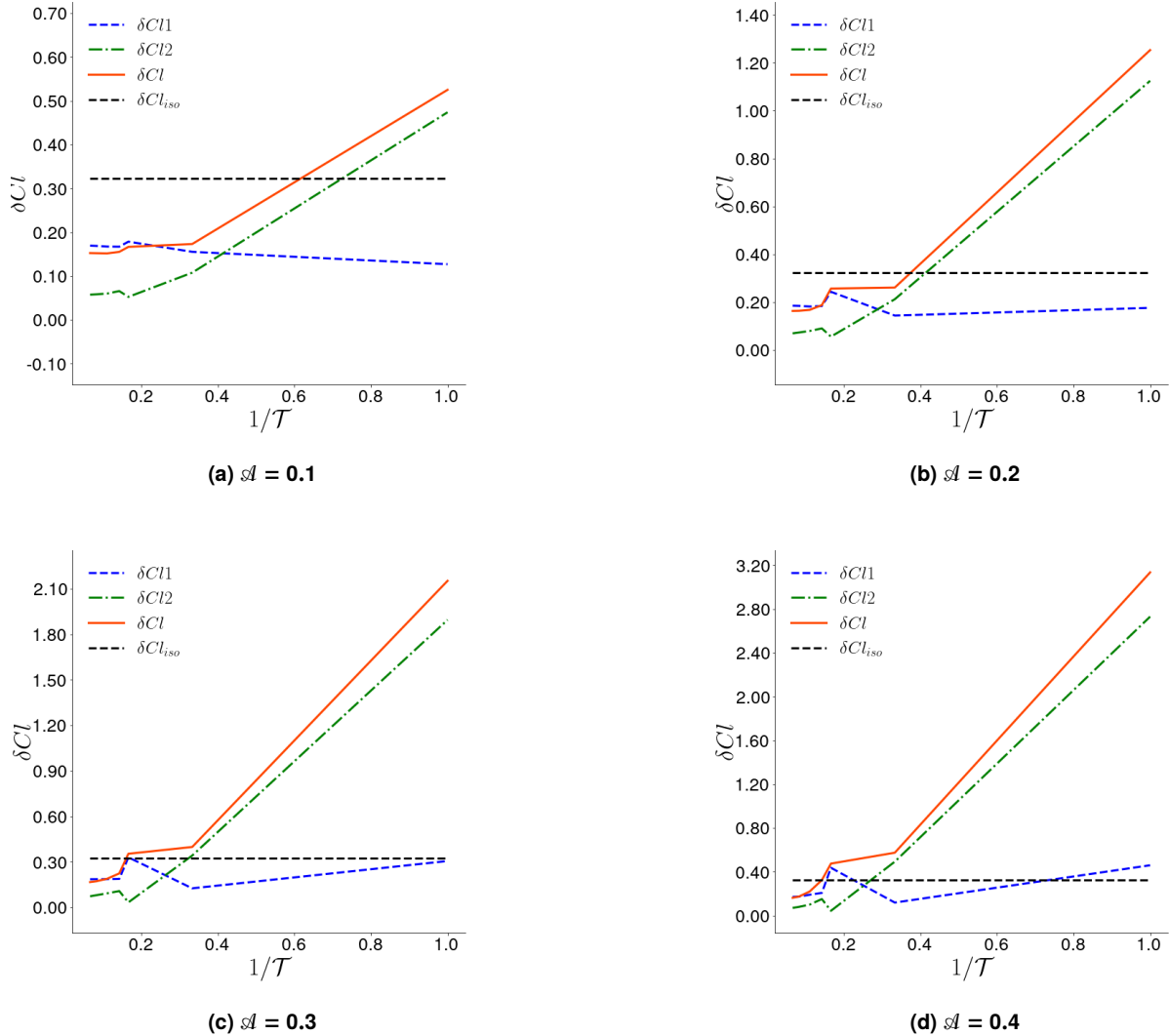


FIGURE 11: Comparison of lift forces fluctuation for the cases with a flapping control rod at $Re = 100$ and $l = 1$

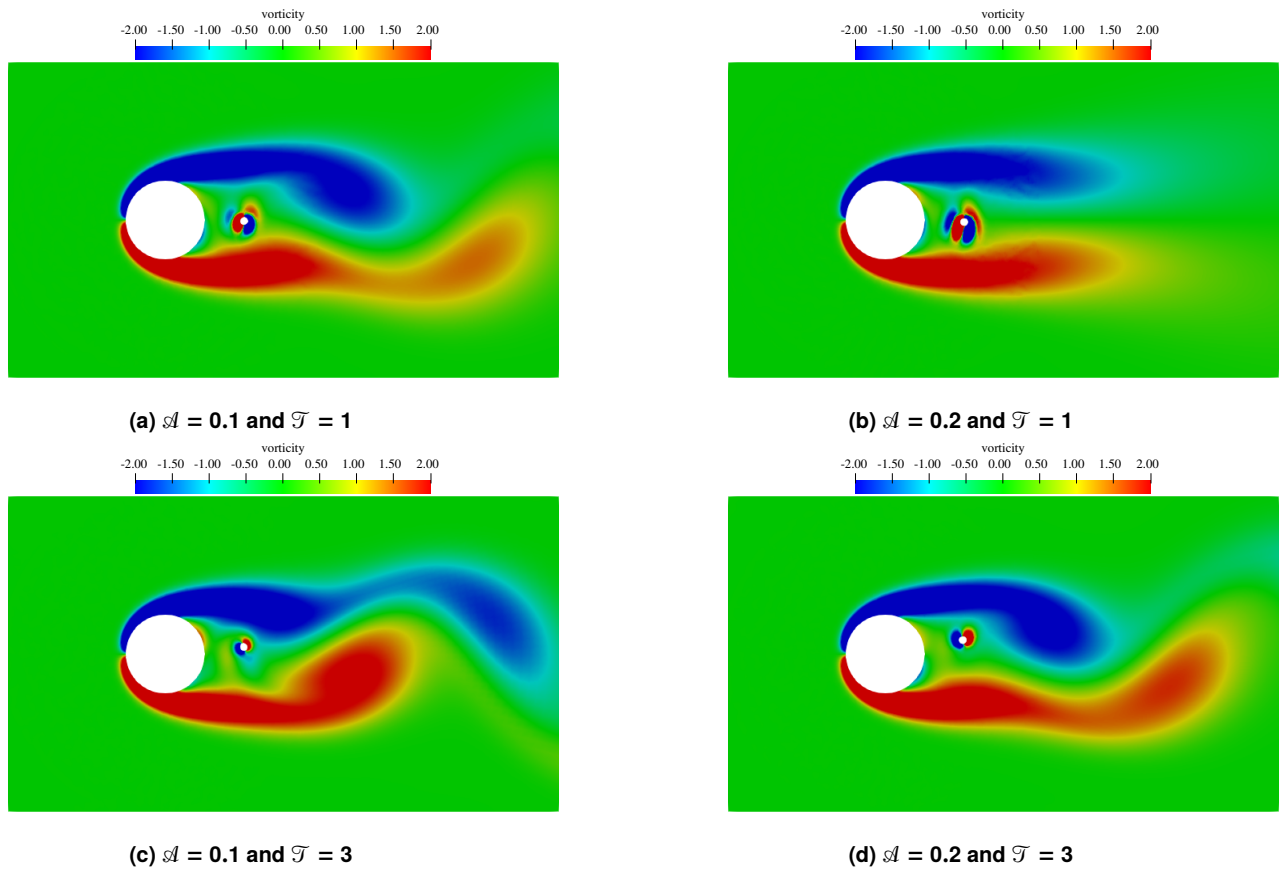


FIGURE 12: Instantaneous contour of vorticity for the cases at $Re = 100$, $I = 0.5$, and $\tau = 400$

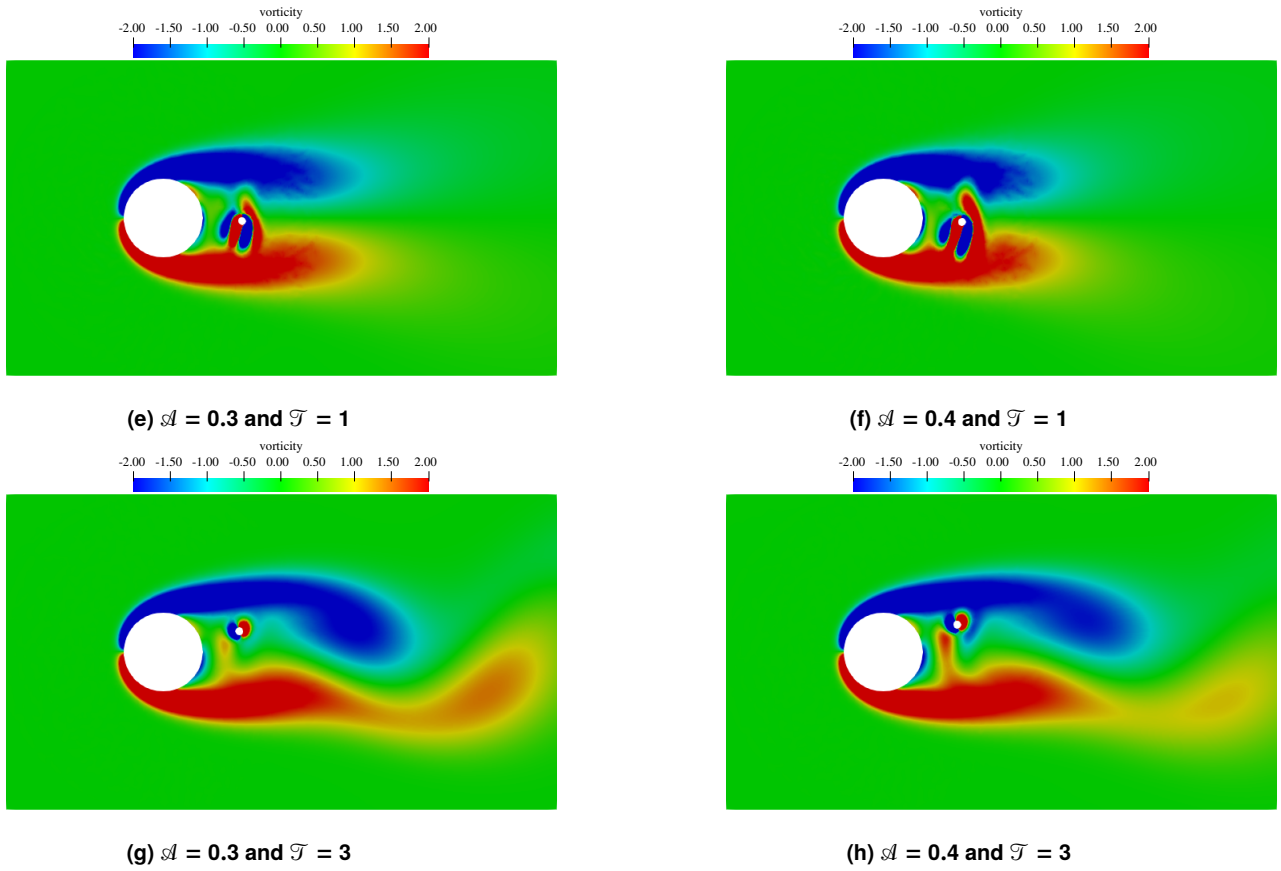


FIGURE 12: Instantaneous contour of vorticity for the cases at $Re = 100$, $l = 0.5$, and $\tau = 400$

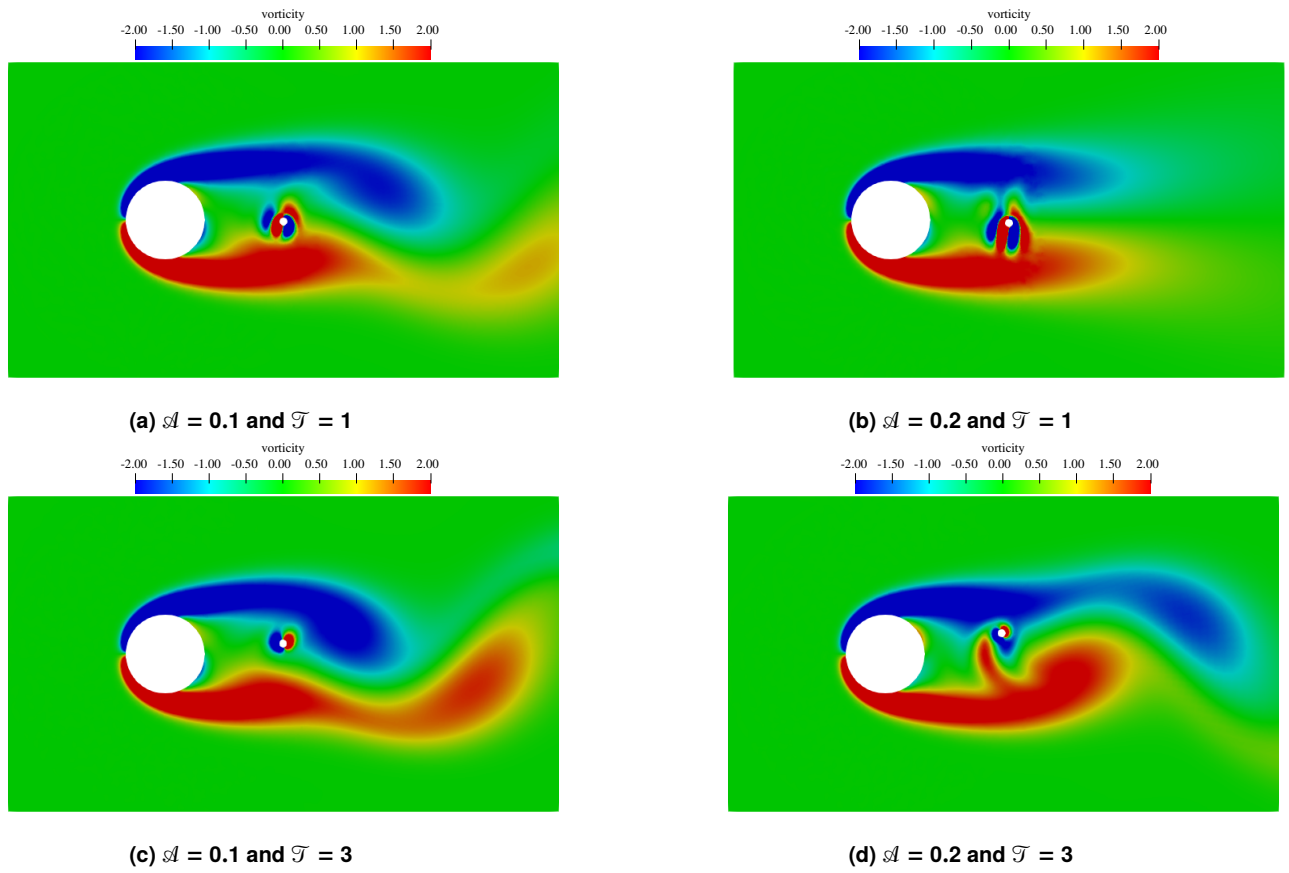


FIGURE 13: Instantaneous contour of vorticity for the cases at $Re = 100$, $l = 1$, and $\tau = 400$

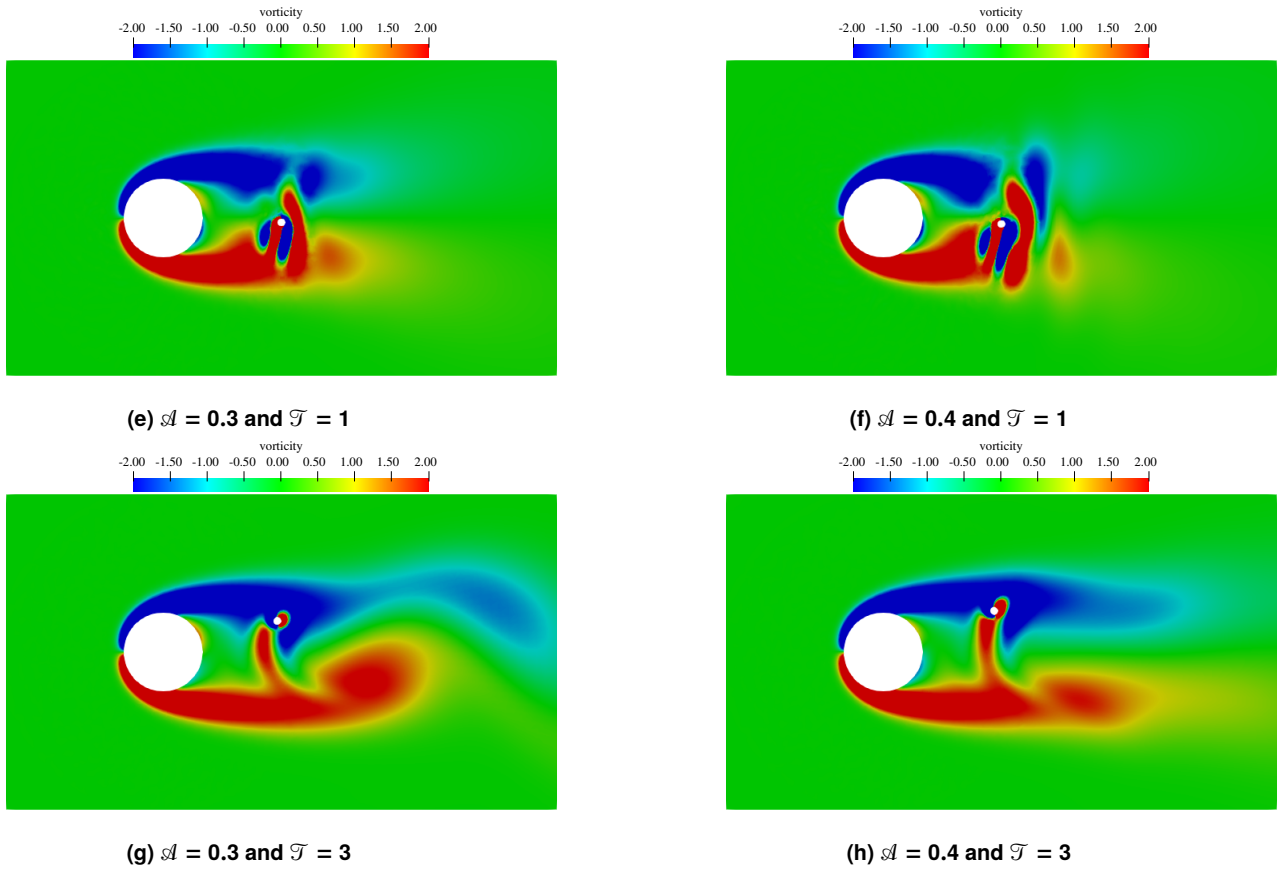


FIGURE 13: Instantaneous contour of vorticity for the cases at $Re = 100$, $I = 1$, and $\tau = 400$

force can be suppressed completely. The same conclusions can be drawn for the cases of a flapping control rod at $l = 1.0$, as shown in Figure 8 and Figure 9. For instance, the mean drag force of cylinder is generally insensitive to the flapping frequency and amplitude, except for the cases of very large flapping amplitude. When the flapping frequency matches with that of lift force, a sudden jump of the mean and fluctuation of lift force can be found; whereas when the flapping frequency matches with that of drag force, the mean and fluctuation of drag force are minimized.

4.3 Effect of a flapping rod on lift forces

By simply placing a stationary control rod in wake, Strykowski & Sreenivasan (1990) [28] and Dipankar & Sengupta, etc. (2004) [30] have found that there is a significant suppression of lift forces over the cylinder. In this study, we found that by placing a stationary control at distance $l = 0.5$ or $l = 1.0$ for the case of $Re = 100$, the lift force can be suppressed by 47%. In this section, it is found that a further suppression of lift force fluctuation can be achieved by flapping the control rod at a particular frequency and amplitude.

In this study, it is found that the fluctuation of lift coefficient of cylinder with a stationary control rod at $l = 0.5$ is about $C_l = 0.17$. By allowing the control rod to flap, Figure 10 and Figure 11 shows that the lift force can be further suppressed if the control rod flaps at $1/\mathcal{T} = 0.33$, approximately the dimensionless frequency of drag force of an isolated cylinder at $Re = 100$. While flapping at $1/\mathcal{T} = 0.33$, the suppression of lift force can reach about 57% in the case of $l = 1.0$. Most importantly, this remarkable results of lift suppression can be achieved at very small flapping amplitude $\mathcal{A} = 0.1$ and consumes a very small amount of actuation energy compared with the setup of flapping plate. A much better result of lift suppression can be achieved by flapping the control rod at $1/\mathcal{T} = 1.0$, in which the efficiency of lift suppression becomes 61%. This efficiency of 61% in the case of $Re = 100$, $l = 1.0$, $\mathcal{A} = 0.1$ and $1/\mathcal{T} = 1.0$ is the best result that can be found in this study, which is also phenomenal.

The vorticity contour also shows lots of insight of this active flow control mechanism. Figure 12 shows the instantaneous vorticity contour for the case of $l = 0.5$. It can be seen in Figure 12b, 12e, and 12f that the vortex shedding is effectively suppressed. Although the flapping control rod is completely encapsulated inside the low-pressure re-circulation region behind the cylinder, as flapping amplitude increases, the strength or shape of the shed vortices are significantly modulated, as shown in Figure 12e, 12f, 12g and 12h.

By placing the control rod further downstream at $l = 1.0$, where the control rod is partially outside the re-circulation region, the effect on suppressing vortex shedding becomes more prominent. While the flapping amplitude $\mathcal{A} \gtrsim 0.2$, Figure 13b, 13d, 13e, 13f, 13g, and 13h show that either the vortex shedding process is completely suppressed or the strength of shed vortices are significantly weakened. It is also found that at this distance, $l = 1.0$, if the flapping amplitude and frequency are large enough, the separated shear layers from the cylinder are completely cut off by the control rod in Figure 13e and 13f.

5. CONCLUSIONS

An active flow control mechanism, flapping control rod, was proposed in this study. The effectiveness of this flow control mechanism was numerically investigated at low Reynolds. It was found that by simply placing a stationary control rod at distance of $l = 0.5$ and $l = 1.0$, the lift force exerted on the cylinder can be reduced by about 47%. If the control rod is allowed to flap in wake, the efficiency of lift suppression could reach 61% in the case of $Re = 100$, $l = 1.0$, $\mathcal{A} = 0.1$ and $1/\mathcal{T} = 1.0$. The advantage is that such a significant lift suppression effect can be achieved at a very small flapping amplitude, which consumes much less actuation power than the setup of flapping plate. It was also noticed that fluctuation of both lift and drag were excited at $1/\mathcal{T} \approx 0.165$, which is about the dimensionless frequency of lift force; and the fluctuation of both lift and drag were minimized at $1/\mathcal{T} \approx 0.33$, which is close to the dimensionless frequency of drag force. In particular, the lift force is further suppressed at a higher frequency $1/\mathcal{T} \approx 1.0$, $\mathcal{A} = 0.1$, and $l = 1.0$, until $\delta C_l \approx 0.122$.

REFERENCES

- [1] Arcara, PC, Bartlett, DW and McCullers, LA. "Analysis for the application of hybrid laminar flow control to a long-range subsonic transport aircraft." Technical report no. SAE Technical Paper. 1991.
- [2] Pechlivanoglou, Georgios. "Passive and active flow control solutions for wind turbine blades." (2013).
- [3] Seshagiri, Amith, Cooper, Evan and Traub, Lance W. "Effects of vortex generators on an airfoil at low Reynolds numbers." *Journal of Aircraft* Vol. 46 No. 1 (2009): pp. 116–122.
- [4] Aider, Jean-Luc, Beaudoin, Jean-François and Wesfreid, José Eduardo. "Drag and lift reduction of a 3D bluff-body using active vortex generators." *Experiments in fluids* Vol. 48 (2010): pp. 771–789.
- [5] Lee, Sang and Loth, Eric. "Supersonic boundary-layer interactions with various micro-vortex generator geometries." *The Aeronautical Journal* Vol. 113 No. 1149 (2009): pp. 683–697.
- [6] Wang, Haipeng, Zhang, Bo, Qiu, Qinggang and Xu, Xiang. "Flow control on the NREL S809 wind turbine airfoil using vortex generators." *Energy* Vol. 118 (2017): pp. 1210–1221.
- [7] Langan, Kevin and Samuels, Jeffrey. "Experimental investigation of maneuver performance enhancements on an advanced fighter/attack aircraft." *33rd Aerospace Sciences Meeting and Exhibit*: p. 442. 1995.
- [8] Farzaneh-Gord, Mahmood and Sadi, Meisam. "Improving vortex tube performance based on vortex generator design." *Energy* Vol. 72 (2014): pp. 492–500.
- [9] Zhou, Guobing and Pang, Mengmeng. "Experimental investigations on thermal performance of phase change material–Trombe wall system enhanced by delta winglet vortex generators." *Energy* Vol. 93 (2015): pp. 758–769.
- [10] Fish, FE and Lauder, George V. "Passive and active flow control by swimming fishes and mammals." *Annu. Rev. Fluid Mech.* Vol. 38 (2006): pp. 193–224.

- [11] Ibrahim, IH and New, TH. "Tubercle modifications in marine propeller blades." *10th Pacific Symposium on Flow Visualization and Image Processing*: pp. 1–11. 2015. Naples Italy.
- [12] Belamadi, Riyad, Djemili, Abdelouahed, Ilinca, Adrian and Mdouki, Ramzi. "Aerodynamic performance analysis of slotted airfoils for application to wind turbine blades." *Journal of wind engineering and industrial aerodynamics* Vol. 151 (2016): pp. 79–99.
- [13] Zeng, Lingwei, Zhao, Fuwang, Wang, Hanfeng, Liu, Yang and Tang, Hui. "Control of flow-induced vibration of a circular cylinder using a splitter plate." *Physics of Fluids* Vol. 35 No. 8 (2023).
- [14] Cui, Guo-Peng and Feng, Li-Hao. "Suppression of vortex-induced vibration of a circular cylinder by a finite-span flexible splitter plate." *Physical Review Fluids* Vol. 7 No. 2 (2022): p. 024708.
- [15] Li, Qin and Liu, Chaoqun. "LES for supersonic ramp control flow using MVG at $M= 2.5$ and $Re= 1440$." *48th AIAA Aerospace Sciences Meeting Including the New Horizons Forum and Aerospace Exposition*: p. 592. 2010.
- [16] Choi, Haecheon, Jeon, Woo-Pyung and Kim, Jinsung. "Control of flow over a bluff body." *Annu. Rev. Fluid Mech.* Vol. 40 (2008): pp. 113–139.
- [17] Cattafesta III, Louis N and Sheplak, Mark. "Actuators for active flow control." *Annual Review of Fluid Mechanics* Vol. 43 (2011): pp. 247–272.
- [18] Amitay, Michael, Pitt, Dale and Glezer, Ari. "Separation control in duct flows." *Journal of Aircraft* Vol. 39 No. 4 (2002): pp. 616–620.
- [19] Corke, Thomas C, Enloe, C Lon and Wilkinson, Stephen P. "Dielectric barrier discharge plasma actuators for flow control." *Annual review of fluid mechanics* Vol. 42 (2010): pp. 505–529.
- [20] Zhao, Ming and Taheri, Erfan. "Control of Flow Past a Circular Cylinder Using a Rotating Control Rod." *Journal of Marine Science and Engineering* Vol. 10 No. 5 (2022): p. 608.
- [21] Schulmeister, James C, Dahl, JM, Weymouth, GD and Triantafyllou, MS. "Flow control with rotating cylinders." *Journal of Fluid Mechanics* Vol. 825 (2017): pp. 743–763.
- [22] Wu, J and Shu, C. "Numerical study of flow characteristics behind a stationary circular cylinder with a flapping plate." *Physics of Fluids* Vol. 23 No. 7 (2011).
- [23] Wu, J, Shu, C and Zhao, N. "Numerical study of flow control via the interaction between a circular cylinder and a flexible plate." *Journal of Fluids and Structures* Vol. 49 (2014): pp. 594–613.
- [24] Wu, J, Qiu, YL, Shu, C and Zhao, N. "Flow control of a circular cylinder by using an attached flexible filament." *Physics of Fluids* Vol. 26 No. 10 (2014).
- [25] Wan, Hui and Patnaik, Soumya S. "Suppression of vortex-induced vibration of a circular cylinder using thermal effects." *Physics of Fluids* Vol. 28 No. 12 (2016): p. 123603.
- [26] Fujisawa, N., Ugata, M. and Suzuki, T. "A study on drag reduction of a rotationally oscillating circular cylinder at low Reynolds number." *Journal of Visualization* Vol. 8 No. 1 (2005): pp. 41–48. DOI [10.1007/BF03181601](https://doi.org/10.1007/BF03181601). URL <http://dx.doi.org/10.1007/BF03181601>. J Vis.
- [27] Prandtl, Ludwig. "Application of the" magnus effect" to the wind propulsion of ships." Technical report no. 1926.
- [28] Strykowski, Pj J and Sreenivasan, Kr R. "On the formation and suppression of vortex 'shedding' at low Reynolds numbers." *Journal of Fluid Mechanics* Vol. 218 (1990): pp. 71–107.
- [29] Modi, VJ. "Moving surface boundary-layer control: A review." *Journal of fluids and structures* Vol. 11 No. 6 (1997): pp. 627–663.
- [30] Dipankar, A, Sengupta, TK and Talla, SB. "Suppression of vortex shedding behind a circular cylinder by another control cylinder at low Reynolds numbers." *Journal of Fluid Mechanics* Vol. 573 (2007): pp. 171–190.
- [31] Sun, Chenlin, Zhou, Tongming, An, Hongwei, Zhu, Hongjun and Cheng, Liang. "On the study of vortex-induced vibration of circular cylinders covered with different roughness." *Applied Ocean Research* Vol. 124 (2022): p. 103215.
- [32] Song, Zhenhua, Duan, Menglan and Gu, Jijun. "Numerical investigation on the suppression of VIV for a circular cylinder by three small control rods." *Applied Ocean Research* Vol. 64 (2017): pp. 169–183. DOI <https://doi.org/10.1016/j.apor.2017.03.001>. URL <https://www.sciencedirect.com/science/article/pii/S0141118716302772>.
- [33] LIU, Ming-Ming, WANG, Hao-Cheng, SHAO, Fei-Fei, JIN, Xin, Tang, Guo-Qiang and YANG, Fan. "Numerical investigation on vortex-induced vibration of an elastically mounted circular cylinder with multiple control rods at low Reynolds number." *Applied Ocean Research* Vol. 118 (2022): p. 102987. DOI <https://doi.org/10.1016/j.apor.2021.102987>. URL <https://www.sciencedirect.com/science/article/pii/S0141118721004491>.
- [34] Hughes, Thomas JR, Franca, Leopoldo P and Balestra, Marc. "A new finite element formulation for computational fluid dynamics: V. Circumventing the Babuška-Brezzi condition: A stable Petrov-Galerkin formulation of the Stokes problem accommodating equal-order interpolations." *Computer Methods in Applied Mechanics and Engineering* Vol. 59 No. 1 (1986): pp. 85–99.
- [35] Brooks, Alexander N and Hughes, Thomas J. R. "Streamline upwind/Petrov-Galerkin formulations for convection dominated flows with particular emphasis on the incompressible Navier–Stokes equations." *Computer methods in applied mechanics and engineering* Vol. 32 No. 1-3 (1982): pp. 199–259.
- [36] Chung, Jintai and Hulbert, GM1223971. "A time integration algorithm for structural dynamics with improved numerical dissipation: the generalized- α method." (1993).
- [37] Jansen, Kenneth E, Whiting, Christian H and Hulbert, Gregory M. "A generalized- α method for integrating the filtered Navier–Stokes equations with a stabilized finite element method." *Computer methods in applied mechanics and engineering* Vol. 190 No. 3-4 (2000): pp. 305–319.

- [38] Liu, Bin. "A Nitsche stabilized finite element method: Application for heat and mass transfer and fluid–structure interaction." *Computer Methods in Applied Mechanics and Engineering* Vol. 386 (2021): p. 114101.
- [39] Liu, Bin and Tan, Danielle. "A Nitsche stabilized finite element method for embedded interfaces: Application to fluid–structure interaction and rigid-body contact." *Journal of Computational Physics* Vol. 413 (2020): p. 109461.
- [40] Stein, Keith, Tezduyar, Tayfun and Benney, Richard. "Mesh moving techniques for fluid–structure interactions with large displacements." *J. Appl. Mech.* Vol. 70 No. 1 (2003): pp. 58–63.
- [41] Liu, Bin and Zhu, Hongjun. "Secondary lock-in of vortex-induced vibration and energy transfer characteristics of a vibrating cylinder subject to cross buoyancy." *Physics of Fluids* Vol. 33 No. 7 (2021).
- [42] Strykowski, Paul John. *The control of absolutely and convectively unstable shear flows*. Yale University (1986).
- [43] Liu, B and Jaiman, RK. "Dynamics and stability of gap-flow interference in a vibrating side-by-side arrangement of two circular cylinders." *Journal of Fluid Mechanics* Vol. 855 (2018): pp. 804–838.
- [44] Liu, Bin and Jaiman, Rajeev K. "Interaction dynamics of gap flow with vortex-induced vibration in side-by-side cylinder arrangement." *Physics of Fluids* Vol. 28 No. 12 (2016).
- [45] Joshi, Vaibhav, Liu, Bin and Jaiman, Rajeev K. "Flow-induced vibrations of riser array system." *International Conference on Offshore Mechanics and Arctic Engineering*, Vol. 49934: p. V002T08A012. 2016. American Society of Mechanical Engineers.
- [46] Zhu, Hongjun, Zhong, Jiawen and Liu, Bin. "Hydro-and thermo-dynamic characteristics of a circular cylinder placed in mixed convection flow." *Physics of Fluids* Vol. 34 No. 9 (2022).
- [47] Zhu, Hongjun, Zhong, Jiawen and Liu, Bin. "Fluid–thermal–structure interaction of three heated circular cylinders in tandem at a low Reynolds number of 150." *Physics of Fluids* Vol. 34 No. 8 (2022).